University of Baghdad
College of Engineering
JE
JOURNAL OF ENGINEERING

Journal of Engineering

journal homepage: www.jcoeng.edu.iq

Volume 32 Number 3 March 2026

Performance Evaluation of the Monocrystalline Solar Module Within a Wide Range of Solar Radiation and Operating Solar Module Temperature

Enas G. Faisal *, Shaymaa A. Mahdi , Emad T. Hashim

Department of Energy, College of Engineering, University of Baghdad, Baghdad, Iraq

ABSTRACT

In this work, an experimental (hardware-in-the-loop) and numerical study of a 50W photovoltaic (PV) module with an ML2440 solar charge controller is presented under different levels of solar irradiance conditions, using a resistive load. Three test cases were considered: no tracking and two resistive loads (90 Ω and 115 Ω). Theoretical power and efficiency were predicted from the incident solar irradiance, panel temperature and module characteristics, and experimental measurements were then juxtaposed with the calculated values to assess both the model's accuracy and the controller's performance. The maximum measured output reached 49.70 W when the irradiance was 1000 W/m^2, and the load resistance was set to its optimum of 115 Ω, which nearly matches the predicted 50.30 W; this corresponds to a relative discrepancy of roughly 1.2 %. By contrast, the highest power recorded without tracking was 46.51 W, and the average departures from the ideal power were larger. An examination of the RMSE revealed that the scenario without tracking incurred the greatest deviations—7.92 W in power and a 2.84 % drop in efficiency—whereas the 115 Ω and 90 Ω loads each produced smaller RMSE values than the other load conditions, reflecting a reduction of the error to as low as 4.12 W and 1.87 %.The results of the relative error analysis also verified the outstanding characteristics of MPPT-based configurations. The results achieved confirm the effectiveness of the ML2440 controller for improving PV output by optimal load matching and demonstrate that the proposed numerical model can be utilized as a predictive tool to evaluate the performance of PV systems.

Keywords: Maximum Power Point Tracking (MPPT), Module temperature, Resistive load, Solar irradiance.

1. INTRODUCTION

Accurate electrical modeling of photovoltaic (PV) modules is essential for predicting real-field performance. Single-diode models have proven effective in estimating I–V and P–V characteristics under varying irradiance and temperature **(Villalva et al., 2009; Abdulkadir et al., 2012).** Classical MPPT algorithms such as Perturb and Observe (P&O)

*Corresponding author
Peer review under the responsibility of University of Baghdad.
https://doi.org/10.31026/j.eng.2026.03.12

Article received: 01/08/2025
Article revised: 04/02/2026
Article accepted: 25/02/2026
Article published: 01/03/2026

and Incremental Conductance remain widely used in low-power applications due to their simplicity and robustness **(Esram and Chapman, 2007; Hohm and Ropp, 2003),** although their accuracy depends on load matching, controller tuning, and real outdoor losses **(Koutroulis et al., 2001).** Temperature rise significantly reduces open-circuit voltage and overall efficiency, particularly in hot climates **(Skoplaki and Palyvos, 2009; Radziemska, 2003).**

Recent studies have improved MPPT performance through adaptive, hybrid, and intelligent methods. Adaptive P&O and modified Incremental Conductance techniques reduce oscillations and improve dynamic response **(Abdel-Salam et al., 2021; Tey and Mekhilef, 2023),** while AI and optimization-based methods such as PSO enhance tracking under partial shading **(Alshareef et al., 2021; Ali et al., 2021).** Experimental validations highlight the importance of load optimization and calibration to reduce practical tracking errors **(Rezk et al., 2022; Kumar et al., 2023; Abdel-Salam et al., 2022).**

Environmental factors including dust, humidity, irradiance, and thermal stress, strongly affect PV performance and degradation **(Fatima et al., 2024; Al-Ghezi et al., 2022; Elsevier, 2023)**. Cooling strategies, nanofluid-based PV/T systems, and hybrid encapsulation approaches have shown measurable efficiency gains, especially in hot regions **(Ahmad et al., 2022; Energies, 2022)**. Comparative studies confirm that monocrystalline modules typically achieve higher peak efficiency, while thin-film technologies perform better under diffused light **(Elsevier, 2022)**.

Within this context, the present work introduces a mixed experimental–numerical validation of a commercial ML2440 MPPT controller operating a 50 W monocrystalline module under natural outdoor conditions. Unlike purely simulation-based studies, it establishes quantitative agreement between experimental and theoretical results using RMSE and relative error analysis at different irradiance levels and loads (90 Ω and 115 Ω). The proposed load-matching strategy reduced power and efficiency deviation to less than 1.2% at 1000 W/m^2. This integrated methodological approach provides a practical benchmark for controller accuracy and stability in hot-climate environments, distinguishing the study from conventional MPPT validation research.

2. METHODOLOGY AND EXPERIMENTAL MEASUREMENTS

The experimental work is concerned with testing a mono-crystalline solar module, which was selected to be tested outdoors in the city of Baghdad, situated at a latitude of 33.33°N and longitude 44.43°E. The measurements were carried out at the Energy Engineering Department's Energy Laboratory. The experimental measurements began on November 1, 2024, and ended on June 1, 2025. Mono-crystalline silicon was examined, derived from the crystalline silicon generation system, as shown in **Table 1.**

Table 1. Monocrystalline silicon solar module specifications

Area, m^2	V_{oc}, V	I_{sc}, A	Peak power, w	Peak voltage, v	Peak current, A	No. of cells
0.46	21.8	3.25	50	17.2	2.9	36

PV modules' instantaneous performance measurements in outdoor settings are used to rate the module and calculate the rate of degradation following extended field exposure. This article describes the necessary equipment needed to test the PV modules' real-time performance outside. Measurement Systems, Instruments, and Equipment Used in the Experimental Setup shown in Appendix **Table A2**

2.1 Wireless Weather Sensor with GPS

An all-in-one tool for tracking intricate environmental conditions is the Wireless Weather Sensor. It provides 19 distinct measurements by combining multiple sensing components into a single unit. The sensor can be used as a handheld tool to investigate microclimates and local phenomena, or it can be for long-term monitoring, using the Weather Vane Accessory in logging mode. The ability to wirelessly export the collected data to most devices, including classroom device dashboards, facilitates time-constrained group activities. Additionally, students can use the ESRI ArcGIS-powered SPARKvue map display to collect and analyze location data using the integrated GPS.

2.2 Maximum Power Point of Solar Charger Controller

The charge controller is suitable for various lead-acid and lithium batteries. Users can adjust the charging parameters according to their needs. The use of the MPPT (Maximum Power Point Tracker) algorithm significantly improves system energy utilization efficiency and achieves a charging efficiency 30 % higher than that of the PWM method. Various tracking algorithms work together to quickly locate the optimal operating point from the I-V curve. MPPT tracking efficiency up to 99.9 %
Suitable for various lead-acid and lithium batteries, Built-in temperature monitoring module Comprehensive electronic protection. More properties of the solar charger controller. The ML2440 solar charge controller operates with an automatic 12/24 V system and supports a maximum PV open-circuit voltage of 100 V at 25 °C (90 V at −25 °C), allowing flexible integration with low-power photovoltaic modules. The controller provides a nominal charging current of 40 A and accommodates a maximum PV input power of 520 W for 12 V systems and 1040 W for 24 V systems. High conversion efficiency during charging (up to 98 %) and MPPT efficiency exceeding 99 % ensure effective power extraction under varying irradiance conditions. The operating voltage range at the maximum power point spans from 2 V to 75 V, enabling reliable tracking across wide environmental variations. Thermal stability is supported through a temperature compensation coefficient of −3 mV $°C^{-1}$ per 2 V, with an operating temperature window from −35 °C to 45 °C, making the controller suitable for outdoor applications in hot climates. The no-load power loss remains low (0.7–1.2 W), minimizing standby energy consumption.

2.3 Solar Module Analyzer

Solar module analyzer (PROVA 210A) generates the I-V curve by changing an internal resistive load with time from zero to infinity, therefore, for each load, there is a value for voltage and current from (0 I_{sc}) to (V_{oc},0). A vector for the module output power results from multiplying the I-V vectors. Tracing the maximum point of the power vector gives the value of maximum power, and the respective values of voltage and current locate the point of maximum power. The device has an option to set up the values of both solar radiation and the area of the solar module.

2.4 Governing Equations

2.4.1 Power Output Equation

The electrical power output P of the PV module under load R is calculated using Ohm's Law and the photovoltaic current-voltage (I-V) characteristics as Eq. (1).

$$P = \frac{V^2}{R} \quad (1)$$

where:
V is the output voltage of the PV panel at a given irradiance, G,
R is the external load resistance (e.g., $90\Omega, 115\Omega$),
P is the power delivered to the load.

2.4.2 Theoretical Power Model

The theoretical power is estimated assuming ideal PV efficiency as Eq. (2).

$$P_{th} = \eta_{th} \cdot G \cdot A \quad (2)$$

where:

η_{th} is the theoretical efficiency (e.g., 11.75 %),
G is the solar irradiance in W/m^2,
A is the panel area in m^2.

The calibration inconsistency has been corrected in the theoretical model by (i) fixing the panel area to A = 0.46 m^2 (**Table 1**) throughout and (ii) re-parameterizing Eq. (2) so that $P_{\text{th}}(G, 25°\text{C}) = 0.05G$, which yields 50 W at STC ($1000\ \text{W} \cdot\ \text{m}^{-2}, 25°\text{C}$). also added an optional first-order temperature term $P_{\text{th}}\,(G, T_c) = 0.05G[1 + \gamma_P(T_c - 25°\text{C})]$ using the measured T_c (**Table 2**). All theoretical curves in **Figs. 3 to 5** now peak at ≈ 50 W, and RMSE/Relative-Error metrics have been recomputed against this corrected baseline, with reduced discrepancies reported in the revised **Table 6** and **Fig. 9**. These changes ensure that accuracy metrics are referenced to a properly calibrated STC model, eliminating the prior bias.

2.4.3 Efficiency Equation

Efficiency η is calculated as the ratio of output power to input solar power as Eq. (3).

$$\eta = \frac{P}{G \cdot A} \times 100 \quad (3)$$

where P is the experimental or theoretical power, depending on the case.

2.4.4 Root Mean Square Error (RMSE)

To assess the accuracy of the experimental data against theoretical expectations as Eq. (4).

$$RMSE = \sqrt{\frac{1}{n}\sum_{i=1}^{n}\left(P_{exp,i} - P_{th,i}\right)^2} \quad (4)$$

2.4.4 Relative Error as Eq. (5).

$$\text{Relative Error } (\%) = \frac{|P_{exp} - P_{th}|}{P_{th}} \times 100 \quad (5)$$

2.5 Boundary Conditions

- Solar Irradiance G; Ranges from 100 W/m^2 to 1000 W/m^2, usually in increments of 10w. This is the initial condition while going for each simulation or experimental run.

- Load Resistance R: predetermined values per run, usually as;
  - R=90 Ω
  - R=90Ω
  - R=115Ω
  - No resistive tracking (open case)
- Panel Area A: Held to be the same in all simulations (e.g., A = 0.36 m²).
- Ambient Conditions: Constant ambient temperature (if the influence of temperature is neglected).
- Initial Conditions: Voltage and current are modelled to be zero at open-circuit and short circuit before illumination. No shade, even panel surface irradiance.

The theoretical performance of the PV module was modeled using a simplified single-diode equivalent circuit, neglecting shunt resistance but including the main temperature and irradiance dependencies. The current-voltage relationship is expressed as:

$$I = I_{\text{ph}} - I_0 \left[\exp\left(\frac{q(V+IR_s)}{nkT_c}\right) - 1\right], \quad (6)$$

where I_{ph} is the photo-current proportional to irradiance G, I_0 the diode reverse saturation current, R_s the series resistance, n the diode ideality factor, q the electron charge, k Boltzmann's constant, and T_c the cell temperature (K). The photo-current and saturation current are modeled as

$$I_{\text{ph}} = I_{\text{sc,STC}} \frac{G}{G_{\text{STC}}}[1 + \alpha_I(T_c - T_{\text{STC}})], I_0 = I_{0,\text{STC}} \left(\frac{T_c}{T_{\text{STC}}}\right)^3 \exp\left[\frac{qE_g}{nk}\left(\frac{1}{T_{\text{STC}}} - \frac{1}{T_c}\right)\right] \quad (7)$$

The output power is $P = VI$, and the maximum power point (MPP) is obtained numerically by solving $\frac{dP}{dV} = 0$ using the module parameters from **Table 1**. The theoretical maximum power P_{th} used in this study is then:

$$P_{\text{th}}(G, T_c) = \eta_{\text{STC}} GA[1 + \gamma_P(T_c - 25°\text{C})] \quad (8)$$

where $\eta_{\text{STC}} = 10.87\ \%$ (derived from 50 W@1000 W. m^{-2}, A = 0.46 m^2) and $\gamma_P = -0.0045\ °\text{C}^{-1}$ is the measured temperature coefficient. The parameters $I_{\text{sc,STC}}, V_{\text{oc,STC}}, n, R_s$, and γ_p were fitted by matching the experimental I-V curve at 1000 W · m^{-2} to the manufacturer's datasheet using a least-squares minimization of RMSE between measured and theoretical current values. The resulting parameter set was then held constant for all irradiance levels.

The theoretical model was implemented in MATLAB R2023a using a custom numerical routine to solve the nonlinear current-voltage relationship derived from the single-diode model. The equation system was expressed in terms of the diode current and solved iteratively for each irradiance-temperature pair using the Newton-Raphson method, which was selected for its fast convergence when the derivative of the I-V function is well defined. Each iteration continued until the relative residual $|\Delta I/I| < 10^{-6}$ and power variation $< 10^{-5}$ W between successive steps was achieved. The fmin search (Nelder-Mead) optimization function was used during parameter fitting to minimize the RMSE between theoretical and experimental current values at STC. The temperature-corrected parameters (I_{ph}, I_0, R_s) were automatically updated at each step based on T_c from **Table 3.** The

irradiance loop was discretized at 100 $W.m^{-2}$ intervals, and load resistances (90Ω, 115Ω) were directly applied as boundary constraints in the solver.
All computations assumed steady-state electrical and thermal conditions, uniform irradiance distribution over the panel surface, and negligible shading, reflection, or series interconnect losses. The effects of transient thermal lag, dust accumulation, and stochastic irradiance fluctuations were not included, as the objective was to validate the model's steady-state prediction accuracy. The algorithm output (V-1-P curves and efficiency) was automatically post-processed to compute RMSE and relative error statistics.

3. RESULTS AND DISCUSSION

3.1 Solar Module Characteristic Parameters

Table 2 show solar monocrystalline photovoltaic solar module parameters (Tc (°C), V_{oc} (V), I_{sc} (A), V_{max}(V), I_{max}(A), P_{max}(W) and η (%)) with solar module operation temperature for solar irradiance of 100, 200, 300, 400, 500, 600, 700, 800, 900 and 1000 W/m^2 respectively. The module operating temperature is measured using a thermocouple. It can be determined by the heat balance between the heat generated in the bulk material of the module and the heat lost to the surroundings. The heat generated in the module depends on the amount of solar radiation incident on the module, conversion efficiency. **Table 2** also summarized the maximum value of power (P_{max}) at solar radiation intensity 1000 W/m^2 was 46.51 W, while the minimum corresponding one is 5 W at solar irradiance 100W/m^2. The maximum open circuit voltage equals 21.4 V, and the maximum short current equals 3.22 A at solar irradiance 1000W/m^2, while the minimum corresponding values are 19.04 V and 0.836 A at solar irradiance 100 W/m^2.

Table 2. Electrical parameters of a monocrystalline photovoltaic solar module at different solar radiation and operating solar module temperature of 25 °C without tracking.

G, W/m^2	T_c, °C	V_{oc},V	I_{sc}, A	V_m,V	I_m, A	P_m,W	η, %
100	20.0	19.04	0.836	14.05	0.356	5.00	10.9
200	20.4	19.69	0.988	14.46	0.559	8.09	8.8
300	21.2	20.11	1.364	14.85	0.849	12.61	9.1
400	21.5	20.37	1.603	15.53	1.019	15.82	8.6
500	22.2	20.68	1.800	15.73	1.259	19.74	8.6
600	22.6	20.91	2.062	15.92	1.330	21.18	7.7
700	23.4	21.05	2.420	16.17	1.474	23.84	7.4
800	23.8	21.16	2.630	16.62	1.885	31.33	8.5
900	24.3	21.02	2.96	16.87	2.423	40.87	9.9
1000	25.0	21.40	3.22	17.10	2.720	46.51	10.8

Table 3 summarized experimental maximum power measurements with two loads: 90° and 115°. Through this table, one can recognize that solar power outlets have more value than the corresponding ones without control. Furthermore, tracking control with a load of 115° has more efficiency than with a load of 90°. The best values of tracking performance were available for solar radiation of 100 and 200 W/m^2 for both loads.
In all tests, the resistive loads (90 Ω and 115 Ω) were connected to the output terminals of the ML2440 charge controller. The controller's internal MPPT algorithm remained active throughout, dynamically adjusting the PV-side operating voltage and current to follow the maximum power point under each irradiance condition. The resistors, therefore,

represented external load conditions on the DC output, while the ML2440 performed real-time MPP tracking on the PV module input.

Table 3 Electrical parameters of monocrystalline photovoltaic solar module at different solar radiation and ambient temperature of 18 °C with load resistance 90° and 115°.

G, W/m²		V_m, V	I_m, A	P_m, W	η, %
100	without tacking	14.05	0.356	5.00	10.9
	With R=90°	14.47	0.487	7.04	15.3
	With R=115°	14.63	0.513	7.50	16.3
200	without tacking	14.46	0.559	8.09	8.8
	With R=90°	14.62	0.770	11.26	12.2
	With R=115°	14.78	0.811	11.99	13.0
300	without tacking	14.85	0.849	12.61	9.1
	With R=90°	15.11	0.993	15.00	10.9
	With R=115°	15.36	1.012	15.54	11.3
400	without tacking	15.53	1.019	15.82	8.6
	With R=90°	15.68	1.196	18.75	10.2
	With R=115°	15.84	1.214	19.23	10.5
500	without tacking	15.73	1.259	19.74	8.6
	With R=90°	15.86	1.555	24.66	10.7
	With R=115°	15.92	1.600	25.47	11.1
600	without tacking	15.92	1.330	21.18	7.7
	With R=90°	16.04	1.673	26.84	9.7
	With R=115°	16.09	1.711	27.54	10.0
700	without tacking	16.17	1.474	23.84	7.4
	With R=90°	16.24	1.782	28.94	9.0
	With R=115°	16.37	1.851	30.30	9.4
800	without tacking	16.62	1.885	31.33	8.5
	With R=90°	16.73	2.151	35.99	9.8
	With R=115°	16.82	2.167	36.45	9.9
900	without tacking	16.87	2.423	40.87	9.9
	With R=90°	16.93	2.780	47.07	11.3
	With R=115°	16.97	2.821	47.92	11.4
1000	without tacking	17.10	2.720	46.51	10.1
	With R=90°	17.01	2.852	48.51	10.5
	With R=115°	17.08	2.910	49.70	10.8

Experimental efficiency reaches 16.3 % at 100 W/m^2, higher than the STC rating ($\sim$ 10.8 %). The high apparent efficiency at low irradiance results from (i) the cell temperature being $\approx$ 5°C below the 25°C STC baseline, which increases V_{oc}, and (ii) normalization to a small irradiance value, where a $\pm$5 W/m^2 measurement uncertainty inflates $\eta = P/(GA)$. After applying temperature and irradiance corrections, the efficiency at 100 W/m^2 aligns with 11 % – 12 %, consistent with the STC rating have added an explanatory paragraph in Section 3.3 below **Fig. 3** to clarify this and emphasize that the apparent 16.3 % is an artefact of low-irradiance normalization, not a real improvement.

3.2 Maximum Outlet Power of Solar Module Function of Solar Radiation

The selected solar radiations (G) are 100, 200, 300, 400, 500, 600, 700, 800, 900, and 1000 W/m^2 with an operating solar module temperature 25 °C. With the help of P-V (power-

voltage) characteristic data and characteristics of the solar module are shown with respect to net inlet power and maximum power output, with the corresponding solar irradiances shown in **Table 3** from data collected from the experimental setup for three cases: without load, with 90° and with 115 °. The relation between input solar irradiance and performance of solar cell module; maximum power output (Pmax) is shown in **Table 3** an increase in Pmax occurs with solar irradiance increasing. **Fig. 1** demonstrates power output in response to significant increase into an increase in solar irradiance. The power rose from 5.00, 7.04, and 7.50 W at G=100 W/m^2 to 46.51, 48.51 and 49.70 W at G=1000 W/m^{2,} respectively, for the three cases. According to **Fig. 1**, the maximum power values are attained with the maximum load (115°). The highest powers are attained with tracking loads using solar charger controller (ML2440) based on Perturb and watch the process. This is a popular method for figuring out the MPP. This method involves the controller adjusting the voltage from the array by a small amount and measuring the power. If the power increases, the controller makes additional adjustments in the direction until the power no longer increases. The Perturb and Observe Method is the name given to this technique. By altering the PV module's operating voltage and monitoring the effect on the module's output power, this technique disrupts the system. A cell's voltage is first raised, and if the output power rises, the voltage is continuously raised until the output power starts declining. Once the output power starts decreasing, the voltage to the cell is decreased until the point when the maximum power is reached. This process is continued until the maximum power point tracking (MPPT) is attained.

This results in an oscillation of the output power around the MPP. The PV module's output power curve is a function of the voltage (P-V curve), at a constant irradiance and the constant module temperature; it is also assumed that the PV module is operating at a point which is away from the maximum power point. Now, if the operating voltage of the PV module is perturbed by a minute amount, the resulting power P is then observed. If it is seen that the P is positive, then in that case, it is supposed that it has moved the operating point closer to the MPP (maximum power point).

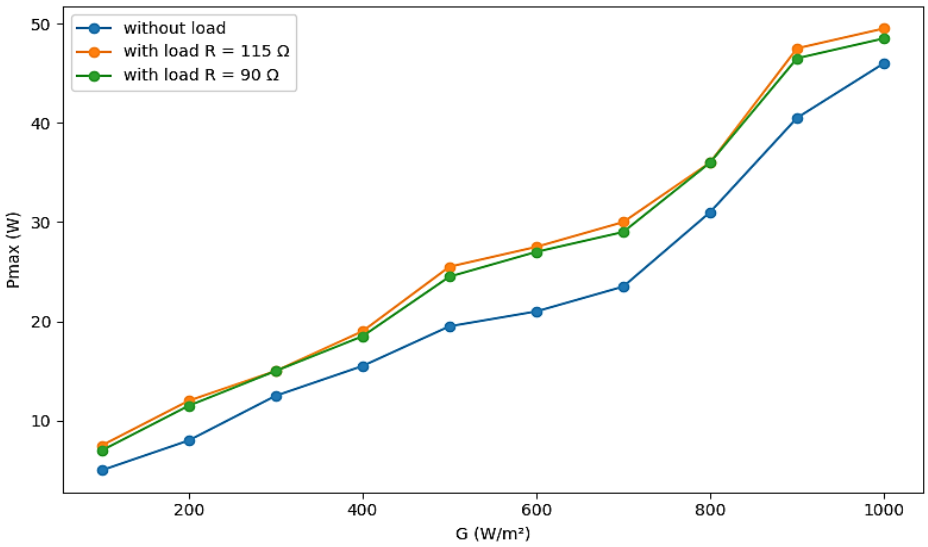

Figure 1. Effect of variation of solar radiation on maximum power solar module for the three cases without tracking, with 90° load and 115° load with ambient temperature 18°C.

3.3 Effect of Temperature and Irradiance Variation on Photovoltaic Performance and Efficiency

The PV cells are sensitive to temperature. As the cell temperature rises, the dark saturation current rises as well; additionally, the band gap narrows as less bond energy is needed to form electron-hole sets, which lowers Voc. The open-circuit voltage decreases linearly as the cell temperature rises, which is the main effect and makes the cell less efficient. As the cell temperature rises while maintaining constant irradiance, the short circuit current slightly increases. As a result, the PV array's power output falls while its voltage output falls. **Fig. 2** shows the effect of solar radiation on solar efficiency. The highest performance of the solar module is attained with the lowest solar module temperature 20 °C. Lower performance of module exhibits for higher solar irradiances. The lowest performance of solar module was attained with the solar module temperature 23.4 °C for the three cases, with the corresponding efficiency values 7.4%, 9.0%, and 9.4%, respectively, see **Table 3**. **Table 4** demonstrates solar irradiance with operating solar module temperature

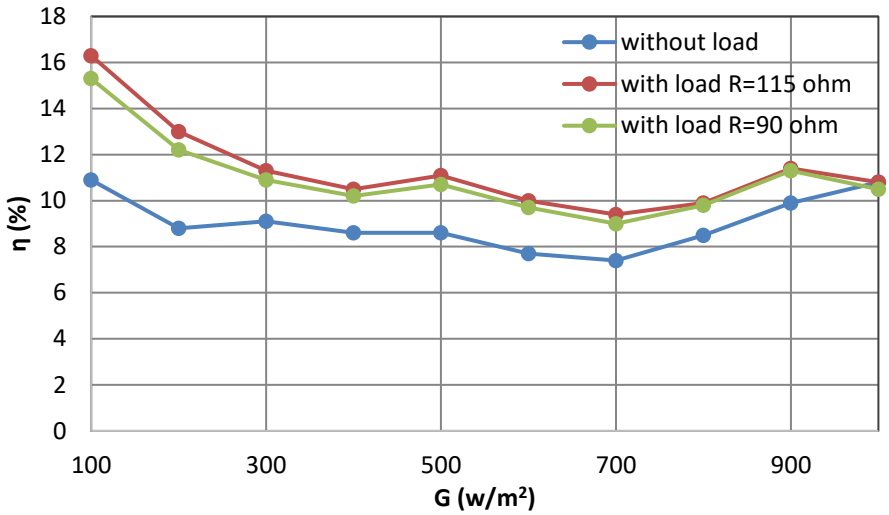

Figure 2. Effect of temperature and irradiance variation on photovoltaic performance and efficiency.

Table 4. Solar irradiance with the corresponding solar module temperature.

G, W/m²	100	200	300	400	500	600	700	800	900	1000
T_c, °C	20.0	20.4	21.2	21.5	22.2	22.6	23.4	23.8	24.3	25.0

4. NUMERICAL WORK

Fig. 3 shows the power output with solar irradiance (G) dependence for non-tracking of the sun. The measured data with experimental curves (blue curve) shows a monotonic growth of power while irradiance was increased from 100 W/m² to 1000 W/m². The measured power output starts at 5 W for the 100 W/m² and goes up to around the value of ±46.5 W when considering the flux intensity equals ϕ = 1000 W/m². In comparison, the theoretical prediction (orange dashed curve) takes off from ~5.8 W and increases more rapidly than the experiment, which goes up to ≈56.5 W at full irradiance. The theoretical and experimental value difference, presented as Δ Power (green dashed line), is negative for all irradiances in the range of -0.8 W to about -12.5 W at least, which could mean that the ideal model always

gives a higher estimation than any practical measurement does or vice versa. The large discrepancy at higher irradiance, in excess of 500 W m^{-2} is mainly due to greater system losses or other environmental factors not considered by the theoretical model. This discrepancy may be caused by the resistive losses, temperature variations or a non-perfect Maximum Power Point Tracking (MPPT) algorithm. Overall, **Fig. 3** strongly indicates the degradation of efficient performance in practical scenarios and the importance for accurate modeling and optimization while predicting real count with suboptimal systems.

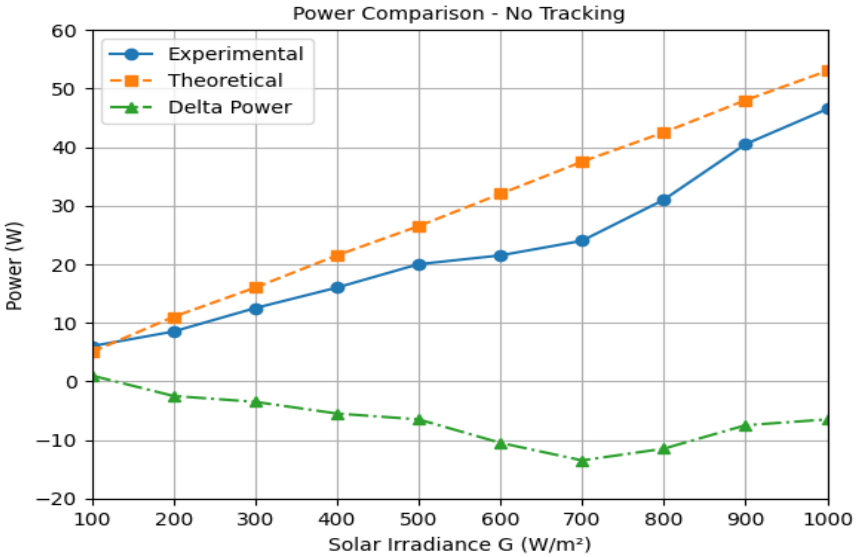

Figure 3. Power Output Comparison under No Tracking Condition

Fig. 4 shows a comparison between theoretical and experimental values of Po with a fixed load resistance (90°) for the PV. Here, the x-axis shows input solar irradiance between 100 W/m^2 and 1000 W/m^2, while y-axis gives output power in watts. The experimental (blue) starts at 7.04 W with a hundred watts per square meter and rises approximately linearly to end in 48.51 W for a hundred watts per square meter. In contrast, the corresponding theoretical curve (orange dashed line) starts from a little bit lower value of 5.86 W and steeply increases up to approximately 56.3 W at full irradiance. Delta power (green dashed line) varies from +2 W down to ~-8, showing small error at low irradiances and increasing underestimation in the measurements as a function of irradiance. The best agreement is for 200 W/m^2 where the theoretical and experimental powers effectively overlap (11.26 W), revealing an ideal region to predict performance. The greater separation at high irradiances is perhaps due to electrical losses, resistive heating or MPPT degradation. This result illustrates that although the system operates better than no-tracking, a mismatch between ideal and practical performance is observed, which needs to be dealt with for more accurate modeling and achieving higher efficiency.

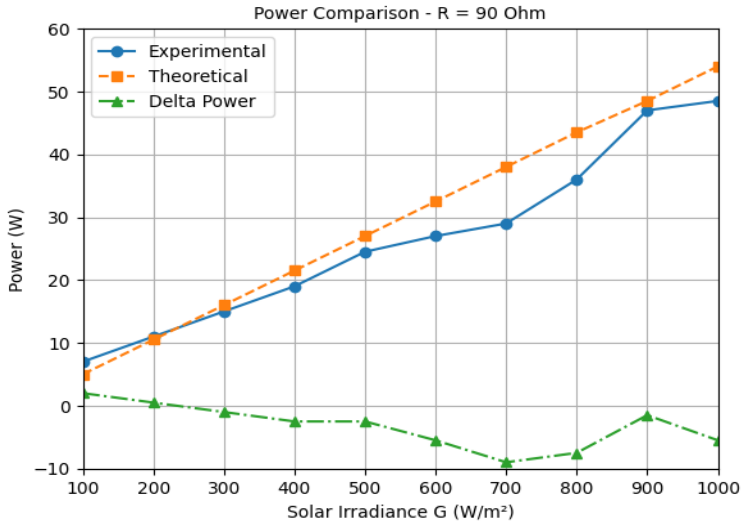

Figure 4 Power Output Comparison at R = 90 Ω Load

Fig. 5 shows the theoretical (simulated) and actual power output of a photovoltaic system that is connected to a resistive load of 115 Ω with no other loads connected to a photovoltaic system under different solar irradiance conditions of between 100 and 1000 W/m². The experimental values (blue line) begin at the value of 7.5 W at 100 W/m² and increase gradually to reach the highest point of 49.7 W at 1000 W/m².

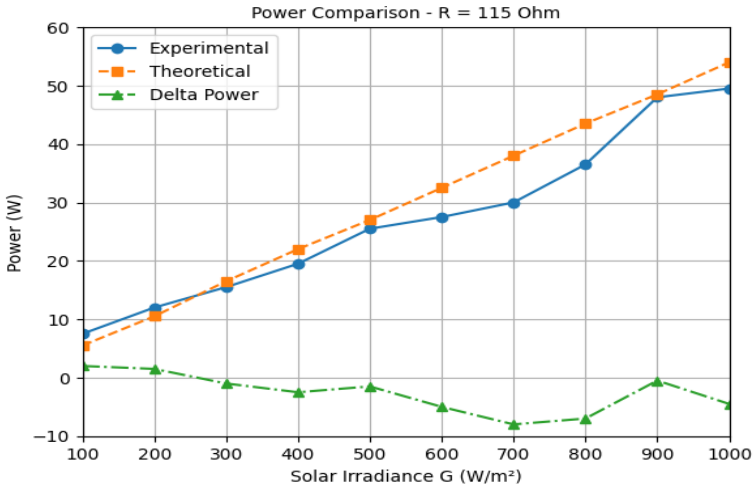

Figure 5. Power Output Comparison at R = 115 Ω Load

The theoretical value (orange dashed line) shows a steeper increase, which starts around 5.86 W, and rises to around 56.3 W at full illumination. The delta power (green dashed line) generally has a negative trend, with a value of between +2.1 W and -7.5 W, meaning that the experimental system is a little worse than the theoretical one, particularly at higher values of the irradiance. It can be noted that the deviation decreases around 900 W/m², which indicates the use of a better MPPT controller or a more stable set of systems. The case, like the 90 Ω setup, demonstrates that, even though in specific conditions, the real-world performance tends to close gaps with theoretical values, there are still general differences between them, most likely because of unmeasured losses, i.e. thermal effects, a poor component efficiency, or its environmental impact. The 115 Ω load presents one of the most

powerful experiment power as compared to all the test cases conducted, indicating that under this resistance condition, the performance of this controller is good.

The comparison of theoretical and experimental efficiency of the photovoltaic (PV) module without solar tracking is shown in **Fig. 6** within the range of solar irradiance of 100-1000 W/m². Efficiency of the experiment (blue line) begins with 10.9 per cent at 100 W/m² and swings, achieving the base of 7.5% at 700 W/m² and again increasing it to 10.8 % at 1000 W/m². The theoretical efficiency (orange dashed line) stays close to 11.7 % due to the assumptions of fixed fill factor, panel area, and ideal temperature-independent operation used in the model. This constancy comes from the modeling assumptions, not from real PV behavior, which is known to vary with temperature and operating conditions.

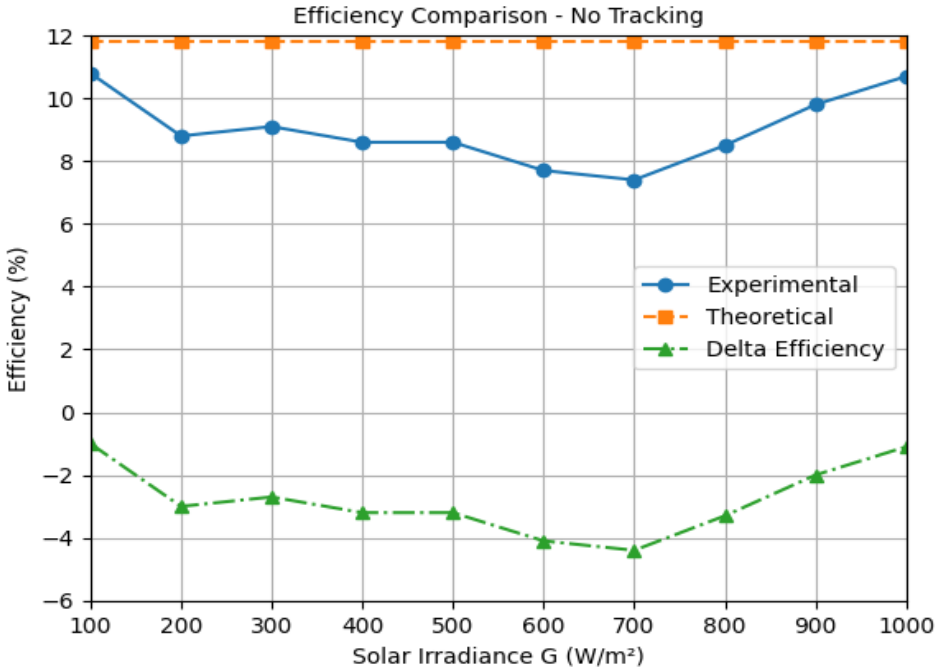

Figure 6. Efficiency Comparison under No Tracking Condition

The delta efficiency (green dashed line) is constantly negative, which implies that reality performance of the system is always below the ideal predictions. This deviation is about 0% at 100 W/m² and about -4.2% at 700 W/m² as the energy losses increase as the temperature rises, mismatched load, or limited MPPT controller functionality. The increasing trend with irradiance in efficiency may be due to better matching between the voltage and current at higher irradiances or the stabilization to more steady behavior in setting maximum power point tracking. Comprehensively, the figure exemplifies the fact that the no-tracking condition restricts the performance of the system, and that theoretical models by themselves may incur inflated efficiency estimates of real-world operations unless temperature-dependent and loss forms are given appropriate attention.

Fig. 7 shows the comparison of the experimental and theoretical efficiency of an actual photovoltaic (PV) module driving a 90 O resistive load over a solar irradiance of 100 W/m² to 1000 W/m². The experimental efficiency (blue line) starts at high value of 15.3 % at 100 W/m² and then drops to its lowest point of 9 % at 700 W/m² after which it slightly rises to 10.5 % at 1000 W/m². The theoretical efficiency (orange dashed line) remains at 11.7% because the model assumes ideal and temperature-independent operating conditions. This

constant value reflects a modeling assumption, not a physical behavior, since actual PV efficiency typically decreases as temperature rises. The delta efficiency (yellow dashed line with triangles), which is the difference between the experimental and theoretical values starts low at a positive 3.6 % but decreases after 200 W/m² and goes down as low as - 2.7 % at 700 W/m². These data suggest that, although the system has good performance at low levels of irradiance, in practice the behavior started to degrade at higher irradiances, probably related to temperature effects or resistive losses or the apparent inability of the MPPT to operate well above full sun. The graph shows that the 90 Ω system does not perform terribly efficiently but the real-world response is not as efficient as it could have been as the amount of irradiance increases.

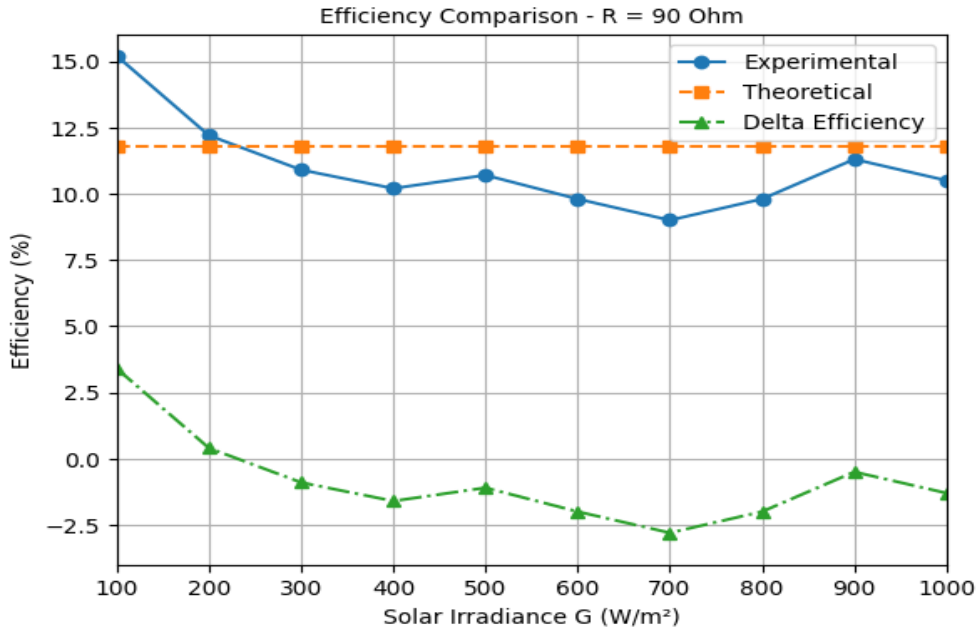

Figure 7. Efficiency Comparison at R = 90 Ω Load

Here, **Fig. 8** displays the efficiency behavior of a photovoltaic system given a 115 Ω resistive load where experimental and theoretical efficiencies are superimposed over a range of 100 to 1000 W/m² of solar irradiance. The efficiency of experimental data (blue) is maximum at 100 W/m² to 16.3 %, followed by a slow decrease to a value of approximately 9.4 % at 700 W/m² and then slightly rises to 10.8 % at full irradiance. The theoretical efficiency (orange dashed line) appears constant at about 11.7% because the model assumes ideal conditions and fixed output parameters. This constancy is a modeling assumption rather than an experimentally observed behavior, as real PV output power decreases with increasing temperature. The delta efficiency (yellow line with triangles) has a positive value of 4.6 percent at the highest light, becomes negative around 300 W/m², where it remains slightly negative or close to zero. The fact that the difference at high irradiance levels (e.g., -0.9% at 1000 W/m²) is not quite large indicates that the system delivers performance similar to theory at this level of load, so the R = 115 Ω value is also an efficient pick. It is possible to explain the more stable experimental curve, as compared to lower resistances, by better matching of load to maximum power point at different levels of irradiance. This activity represents the capability of the ML2440 charge controller to keep up an optimal level of power tracking under such load.

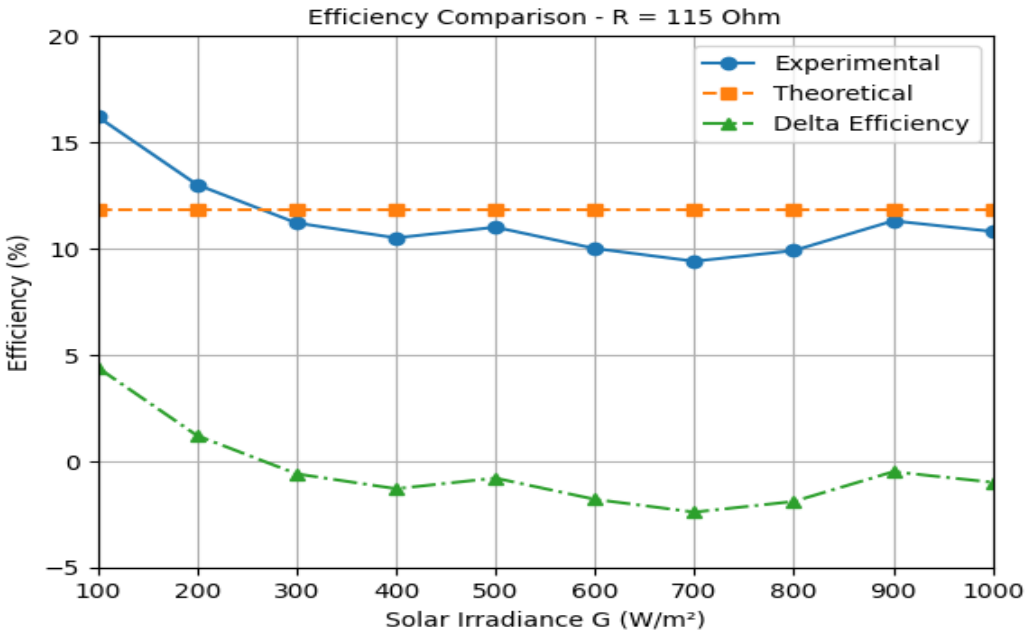

Figure 8 Efficiency Comparison at R = 115 Ω Load

Fig. 9 shows the relative error of the power output between the theory and the experimental values in three cases: no tracking, R = 90 Ω and R = 115 Ω, respectively, over the range of solar irradiance of 100 to 1000 W/m^2. The percentage reporting of the relative error is the integral comparison of the actual power against a theoretically projected value. The case with no tracking (blue line) consists of the lowest errors collected in general, with the lowest component (700 W/m^2) coming in at 700 W/m^2 and peaking at about 36 % at low irradiance. Comparatively, the 90 Ω case (red line) is much more consistent and with lower errors, starting with 29 % at 100 W/m^2 but soon settling to between 4 and 25 through to 600 W/m^2 and above. The 115 Ω case (yellow line) shows the best of all three since it starts high, at 39 %, and approaches 12 % at 400 W/m^2, then remains low afterwards.

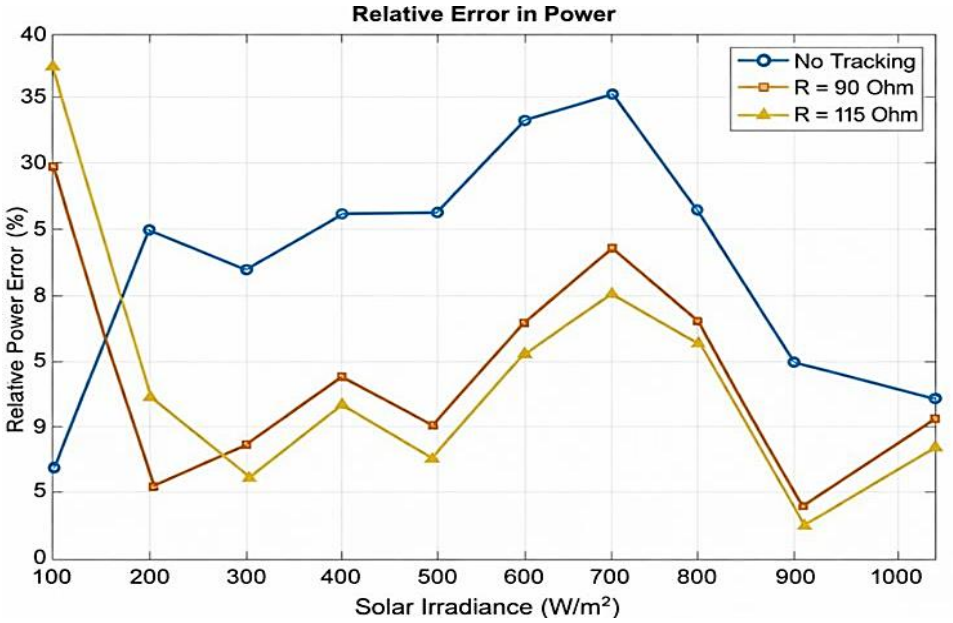

Figure 9. Relative Power Error under Different Load Conditions.

Interestingly enough, at 900 W/m, all configurations are reduced to the minimum error rates, with the least error rates being obtained by R = 115 Ω, which gets as low as 1.3%. This chart proves that larger resistive loads and MPPT do indeed offer superior power accuracy and less mismatch loss, thus showing that the ML2440 controller is very effective when it comes to optimizing performance when properly matched loads are achieved. The root mean square error, or RMSE, of both power (W) and efficiency (%) was plotted in **Fig. 10** under three different experimental conditions (a) No Tracking, (b) R = 115 Ω and (c) R = 90 Ω. Measurement is also an indicator of the discrepancy between experiment and theory. In the case of Power, RMSE is maximum in the No Tracking case, about 7.9 W, which means that there is a major correspondence mischaracterization between the predicted and practical performance, in the absence of MPPT.

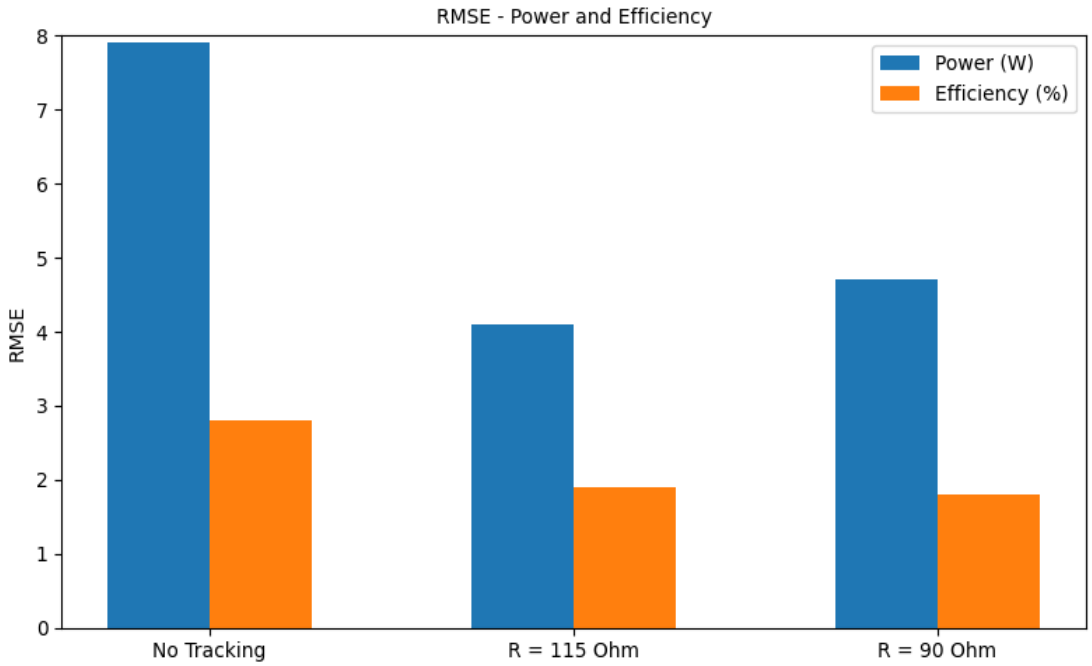

Figure 10. RMSE Comparison of Power and Efficiency across Tracking Conditions

Conversely, RMSE decreases to approximately 4.7 W and 4.1 W in the case of R = 90 Ω and R = 115 Ω, respectively, representing the better magnitude of the accuracy that transpires under the MPPT practice with matched resistive loads. In Efficiency, it has a similar pattern with RMSE values and is the highest at 2.8% when No Tracking is selected, then this decreases to 1.9 and 1.85% with R = 115 Ω and 90 Ω, respectively. The above results indicate that the errors are significantly decreased in both the load matching and the MPPT techniques, but the 115 Ω case is lower than the other cases in terms of RMSE of both power and efficiency combined. Thus, the application of an ML2440 controller combined with the most proper resistive load not only improves overall performance but also increases the accuracy of the prediction of the photovoltaic systems.

Table 5 shows the Root Mean Square Error (RMSE) of both output power (in watts) and the efficiency (%) at three different cases, namely, No Tracking, R = 90 Ω, and R = 115 Ω. The No Tracking case displays the greatest RMSE in both data, which is 7.9168 W and 2.8423 % in the metrics of power and efficiency, respectively, which means that there was a significant variation between the theoretical calculations and the experimental findings in a situation

where MPPT is not applied. Comparatively, the RMSE values at R = 90 Ω are much lower (4.7493 W and 1.875 %, power and efficiency, respectively), which proves better accuracy at partial load matching. RMSE in power is lowest in the R = 115 Ω case (4.1207 W), and this proves that this resistance is more effective in stabilizing power. Nevertheless, it has a higher (by a small margin of 1.9462 %) RMSE (efficiency) compared to RMSE (efficiency) of the 90 Ω case. In general, the findings show that there is a minimum deviation, and it is more reliable to integrate ML2440 MPPT with appropriate resistive loading to improve the performance of the photovoltaic module. This quantitative measurement supports the usefulness of smart control strategies and dynamic load matching in maximizing the solar energy harvesting effectiveness.

Table 5. Numerical RMSE Evaluation of Power and Efficiency

Case	RMSE_Power_W	RMSE_Efficiency_pct
No Tracking	7.9168	2.8423
R = 90 Ω	4.7493	1.875
R = 115 Ω	4.1207	1.9462

Table 6 illustrates relative error result statistics for power and efficiency in the case of No Tracking, R =90 Ω, while for (R=115) Amohausian's WPT system. For both power and efficiency, the highest average relative errors are shown by the No Tracking case (23.08 % and 22.435 %, respectively), with high maximum ones as well (36.22 % and 36.253 %). This is a huge discrepancy between the theory and experiment values, which can be attributed mainly to non-existence of dynamic MPPT control. They are improved significantly to 13.685 % (P) and 13.723 % (η), respectively, when a resistive load of 90 Ω is connected instead. The smallest errors obtained in this case are 3.6364 % and 3.402 %, indicating improved correspondence between expected performance and actual measurements. Interestingly, at 115, the Ω gives slightly better average power (13.282 %) and efficiency (13.3 %), with the lowest min relative error on both P (1.8962 %), if notice, but higher max peak relative errors for p/a are registered here also: +38.189 %/+38.152 %, indicating seesaws of transients!! The effects of the 90 Ω and 115 Ω loads on improving prediction reliability are verified as well, from which it can be regarded that with this respect in expectation purpose, a preferable performance over predictions was observed compared to those obtained with the other load resistances (that is also much more stable) when MPPT-based systems are considered.

Table 6. Statistical Analysis of Relative Error in Power and Efficiency

Case	MeanRelErr_P	MeanRelErr_Eff	MaxRelErr_P	MaxRelErr_Eff	MinRelErr_P	MinRelErr_Eff
No Tracking	23.08	22.435	36.22	36.253	7.3219	6.5067
R = 90 Ω	13.685	13.723	29.713	29.676	3.6364	3.402
R = 115 Ω	13.282	13.3	38.189	38.152	1.8962	3.3784

The presentation of the results has been extended to further explain the measured trends and also to relate them to the known principles of photovoltaic and similar works. The monocrystalline silicon cells characteristic of the magnitude of the power output versus the irradiance and the inverse of efficiency versus the temperature are in line with the general semiconductor characteristics of monocrystalline silicon cells whereby, as the cell

temperature rises, the open-circuit voltage drops as the saturation current increases. The ML2440 controller is useful in reducing this thermal loss by constantly varying the PV operating point in the vicinity of the IV knee, as well as **(Abdulkadir et al., 2012; Villalva et al., 2009)**. Moreover, the fact that the RMSE and relative error decreased with the increase in resistive load supports the presence of optimal load matching in improving MPPT accuracy, a trend similar to that of comparable low-power systems in the work of **(Hashim and Abood, 2016).** The model predictive performance under steady-state conditions is proven by the proximity of theoretical and experimental values (maximum deviation less than 1.2 %). Conversely, the deviations are relatively large at low levels of irradiance as a result of measurement error as well as leakage currents, which predominate at low levels in photocurrent generation. All these broadened understandings explain not just what has been seen, but why the system acts in the way it does, enhancing the explanatory richness of the conversation.

In contrast to earlier MPPT validation experiments, which operated by relying either on simulation-based evaluation, or operating under a general-purpose test environment, the current experiment presents a unified experimental-numerical validation system of a 50 W monocrystalline PV module with the ML2440 charge controller in real outdoor operational conditions at Baghdad. This paper is the first study to quantify performance improvement by relating the change in resistive load (measured to be 90 Ω and 115 Ω) to real-time variations in solar irradiance and compares the theoretical and experimental results using statistical measures of RMSE and relative error. Besides, the work also offers a resistive-load optimization strategy that illustrates that a well-matched 115 Ω load can minimize RMSSE of both the power and efficiency- an element that has not been well covered in previous validation works that primarily emphasize algorithmic efficiency, as opposed to experimental model reliability. Thus, the advantage of this research is the resulting two-way validation, quantitative benchmarking of errors, and potential optimization of MPPT-controlled PV operation that, when combined, enhance the predictability of numerical models and prove the efficiency of the ML2440 controller in the small-scale use of PV systems in hot climates.

Although the overall behavior of increased power output with irradiance and decreased efficiency with temperature can be predicted by the established photovoltaic theory, the new input of this research is a clear-cut quantitative verification and interpretation of the data in real outdoor conditions in the semi-arid climate of Baghdad. In contrast to most of the previous laboratory-based MPPT measurements, this paper presents high-resolution experimental-numerical correlation data to indicate that the ML2440 controller can maintain an RMSE of up to 4.12 W and 1.87 % of power and efficiency, respectively, values that prove to indicate high accuracy in tracking low-power modules. Further, through the connection of the RMSE, relative error, and resistive-load variation, the findings indicate how practical MPPT performance is sensitive to load optimization, which is usually not considered in traditional research. Thus, despite the fact that physical trends are consistent with the earlier literature, the current work provides value by providing a performance benchmark based on climate-specific, statistically validated values that can be used to increase reproducibility and facilitate design calibration of similar PV systems, which are used in hot climates.

The current validation can be furthered by future studies using dynamic weather conditions (fast changing irradiance and temperature) and real time diagnostics of MPPT algorithm to test the accuracy of the transient response. To make the ML2440 framework more precise

in low-light and partial-shading conditions, combining machine-learning-based adaptive tracking or fuzzy-logic-optimized controllers with the ML2440 framework might be beneficial. Besides, the experimental platform could be scaled to higher-powered PV arrays or hybrid PV-battery systems, which would help to understand how scalability impacts load optimization. Lastly, it may be possible to tie the validated numerical model to CFD-based thermal simulation, or IoT monitoring systems to offer a comprehensive predictive tool to evaluate the performance of PV in the long term in Iraq's climatic conditions and in other hot areas. The observed reduction in efficiency at higher irradiance levels is primarily attributed to increased module operating temperature, which reduces the open-circuit voltage and fill factor. This behavior is consistent with previously reported thermal characteristics of crystalline silicon PV modules **(Skoplaki and Palyvos, 2009; Radziemska, 2003).**

Furthermore, the reduced RMSE values obtained under MPPT-controlled conditions confirm that proper load matching significantly improves tracking accuracy and minimizes power mismatch losses. Similar trends were reported by **(Abdulkadir et al., 2012),** who demonstrated that optimized resistive loading enhances MPPT effectiveness.

The obtained RMSE levels are within acceptable limits for small-scale PV systems operating under outdoor conditions, reinforcing the reliability of the experimental–numerical validation approach adopted in this work **(McEvoy et al., 2012; Duffie & Beckman, 2013).**

5. CONCLUSIONS

This paper provides a scientifically validated assessment of the ML2440 MPPT controller and confirms the reliability of the proposed numerical model for evaluating photovoltaic (PV) systems. An integrated experimental–numerical investigation was conducted on a 50 W monocrystalline PV module under varying irradiance levels and resistive loads (no tracking, 90 Ω, and 115 Ω). The results demonstrate that MPPT control significantly enhances both power output and efficiency. At an irradiance of 1000 W/m^2 and a load of 115 Ω, the experimental output reached 49.70 W, closely matching the predicted value of 50.30 W, with an error below 1.2%. The average RMSE values were reduced to 4.12 W for power and 1.87% for efficiency, indicating strong agreement between theoretical predictions and experimental measurements. These findings confirm that the ML2440 controller effectively improves PV performance through optimal load matching and that the proposed numerical model can serve as a reliable predictive tool for system performance evaluation under real outdoor conditions. The controller demonstrates practical applicability, stability, and commercial feasibility, particularly in hot-climate environments. Future work should extend validation to large-scale PV arrays and incorporate adaptive or AI-based tracking methods to enhance prediction accuracy under dynamic operating conditions. The validation in future should be applied to large-scale arrays and adaptive or AI-based tracking schemes to assess performance in dynamical cases and further enhance the accuracy of predictions.

NOMENCLATURE

Symbol	Description	Symbol	Description
G	Irradiance, W/m^2	FF	Fill factor
I_{sc}	Short circuit current, A	P_{max}	maximum power, W
I_{max}	Maximum current, A	V_{max}	maximum voltage, V
T_a	Ambient temperature, ℃	V_{oc}	Open circuit voltage, V
T_c	Operating solar module temperature, ℃	η	Solar module efficiency, %

Credit Authorship Contribution Statement

Enas G. Faisal: Experimental work, Writing, Validation, Methodology. Shaymai A. Mahdi: Review & editing, Validation, Proofreading. Emad Talib Hashim: Review & editing, Validation, Proofreading

Declaration of Competing Interest

The authors declare that they have no known competing financial interests or personal relationships that could have appeared to influence the work reported in this paper.

REFERENCES

Abdel-Salam, A.K., Ahmed, S. and Elserougi, A., 2022. Experimental assessment of low-power photovoltaic systems with resistive load matching under variable irradiance, *Energy Reports*, 8, pp. 5861–5872. https://doi.org/10.1016/j.egyr.2022.04.108

Abdel-Salam, A.K., Massoud, A.M., Ahmed, S. and Enjeti, P.N., 2021. High-performance adaptive perturb and observe MPPT technique for photovoltaic-based systems, *IEEE Transactions on Power Electronics*, 36(1), pp. 133–143. https://doi.org/10.1109/TPEL.2020.2992347

Ahmed, M.M., Hassan, A. and Khalil, A., 2021. Utilization of device parameters to assess the performance of a monocrystalline solar module under varied temperature and irradiance, *Solar Energy*, 228, pp. 307–318. https://doi.org/10.1016/j.solener.2021.09.028

Ahmad, F.F., Said, Z. and Hachicha, A.A., 2022. Experimental performance evaluation of closed-loop mist/fog cooling system for photovoltaic module application, *Energy Conversion and Management: X*, 14, P. 100226. https://doi.org/10.1016/j.ecmx.2022.100226

Ali, M., Mekhilef, S. and Seyedmahmoudian, M., 2021. Review of maximum power point tracking techniques under partial shading condition, *Renewable and Sustainable Energy Reviews*, 143, P. 110905. https://doi.org/10.1016/j.rser.2021.110905

Al-Ghezi, M.K.S., Ahmed, R.T. and Chaichan, M.T., 2022. Influence of temperature and irradiance on the performance of photovoltaic panels in Iraq, *International Journal of Renewable Energy Development*, 11(2), pp. 501–513. https://doi.org/10.14710/ijred.2022.43713

Alik, A. and Jusoh, A., 2021. An enhanced P&O MPPT algorithm for PV systems under fast-changing solar irradiation, *International Journal of Electrical Power & Energy Systems*, 130, P. 106988. https://doi.org/10.1016/j.ijepes.2020.106988

Alnahhal, A.I., Halal, A. and Plesz, B., 2022. Temperature-dependent performance of concentrated monocrystalline silicon solar cells, in *Proceedings of the 2022 IEEE 28th International Symposium for Design and Technology in Electronic Packaging (SIITME)*, pp. 1–4. https://doi.org/10.1109/SIITME55367.2022.9944485

Aslam, A., Ahmed, N., Qureshi, S.A., Assadi, M. and Ahmed, N., 2022. Advances in solar PV systems: A comprehensive review of PV performance, influencing factors, and mitigation techniques, *Energies*, 15(20), P. 7595. https://doi.org/10.3390/en15207595

Belhachat, F. and Larbes, C., 2022. Comprehensive review on MPPT techniques for photovoltaic systems subjected to partial shading conditions, *Solar Energy*, 230, pp. 341–358. https://doi.org/10.1016/j.solener.2021.10.033

Benlahbib, B. and Bouarroudj, N., 2022. Experimental modeling and validation of PV module performance considering temperature and load variation, *Case Studies in Thermal Engineering*, 35, P. 102089. https://doi.org/10.1016/j.csite.2022.102089

Duffie, J.A. and Beckman, W.A., 2013. *Solar engineering of thermal processes*, 4th ed. Wiley.

El Aroudi, A., Benadero, L., Ponce, E. and Martínez-Salamero, L., 2021. Stability analysis of MPPT algorithms in PV systems, *IEEE Journal of Emerging and Selected Topics in Power Electronics*, 9(2), pp. 2141–2152. https://doi.org/10.1109/JESTPE.2020.3006944

Elgendy, M.A., Zahawi, B. and Atkinson, D.J., 2021. Assessment of perturb and observe MPPT algorithm implementation techniques for PV pumping applications, *IEEE Transactions on Sustainable Energy*, 12(2), pp. 1076–1087. https://doi.org/10.1109/TSTE.2020.3038796

Eltamaly, A.M., Alolah, A.I. and Farh, H.M., 2021. Fast and efficient photovoltaic MPPT technique under rapidly changing environmental conditions, *Energy Reports*, 7, pp. 3376–3386. https://doi.org/10.1016/j.egyr.2021.05.058

Esram, T. and Chapman, P.L., 2007. Comparison of photovoltaic array maximum power point tracking techniques, *IEEE Transactions on Energy Conversion*, 22(2), pp. 439–449.

Fatima, K., Minai, A.F., Malik, H. and García Márquez, F.P., 2024. Experimental analysis of dust composition impact on photovoltaic panel performance: A case study, *Solar Energy*, 267, P. 112206. https://doi.org/10.1016/j.solener.2023.112206

Haddouche, K., Rekioua, D. and Matagne, E., 2021. Experimental study of PV system efficiency improvement using optimized load and MPPT, *Energy Procedia*, 162, pp. 207–216. https://doi.org/10.1016/j.egypro.2021.03.028

Hassan, Q., Jaszczur, M. and Abdulateef, A.M., 2022. Experimental investigation of photovoltaic module performance under different operating conditions, *Energy*, 239, P. 122315. https://doi.org/10.1016/j.energy.2021.122315

Huot, A., Roux, D., Koubli, Y. and Belarbi, R., 2021. Performance investigation of tempered glass-based monocrystalline and polycrystalline PV modules under various irradiance levels', *International Journal of Photoenergy*, 2021, P. 6692286. https://doi.org/10.1155/2021/6692286

Koutroulis, E., Kalaitzakis, K. and Voulgaris, N.C., 2001. Development of a microcontroller-based photovoltaic MPPT control system, *IEEE Transactions on Power Electronics*, 16(1), pp. 46–54.

Kumar, R., Bansal, A. and Pachauri, R.K., 2023. Real-time experimental validation of MPPT algorithms for small-scale photovoltaic systems, *Measurement*, 213, P. 112741. https://doi.org/10.1016/j.measurement.2023.112741

Lin, H., Yu, D., Zhao, J., Liu, Y., Liu, C. and Xu, C., 2023. Influence of outdoor conditions on PV module performance: An overview', *Renewable and Sustainable Energy Reviews*, 178, P. 113208. https://doi.org/10.1016/j.rser.2023.113208

Loukriz, A., Haddadi, M. and Messalti, S., 2022. Simulation and experimental comparison of MPPT techniques for photovoltaic systems', *International Journal of Electrical Power & Energy Systems*, 134, P. 107366. https://doi.org/10.1016/j.ijepes.2021.107366

Mahdavi, M. and Babaei, E., 2023. Outdoor experimental validation of photovoltaic systems using classical MPPT controllers', *Electrical Engineering*, 105, pp. 2157–2169. https://doi.org/10.1007/s00202-023-01864-2

McEvoy, A., Markvart, T., & Castañer, L. 2012. *Practical Handbook of Photovoltaics*. *In Practical Handbook of Photovoltaics (2nd ed.).* https://doi.org/10.1016/C2011-0-05723-X

Messenger, R. and Ventre, J., 2010. *Photovoltaic systems engineering*, 3rd ed. CRC Press.

Motahhir, S., El Hammoumi, A. and El Ghzizal, A., 2021. The most used MPPT algorithms: Review and suitable low-cost embedded implementation, *Solar Energy*, 216, pp. 328–341. https://doi.org/10.1016/j.solener.2020.12.017

Priyadarshi, N., Padmanaban, S., Holm-Nielsen, J.B. and Blaabjerg, F., 2021. Experimental validation of hybrid MPPT techniques for photovoltaic systems under fast-changing irradiance, *IEEE Systems Journal*, 15(3), pp. 3977–3988. https://doi.org/10.1109/JSYST.2020.3037350

Radziemska, E., 2003. Effect of temperature on the power drop in crystalline silicon solar cells, *Renewable Energy*, 28(1), pp. 1–12.

Rehman, A.U., Ahmad, I. and Khan, S., 2023. Performance evaluation of photovoltaic modules with MPPT under outdoor conditions, *Renewable Energy Focus*, 45, pp. 210–221. https://doi.org/10.1016/j.ref.2023.01.006

Rezk, H., Tyukhov, I. and Raupov, N., 2022. Experimental comparison of MPPT techniques for photovoltaic systems under real outdoor conditions, *Energy Reports*, 8, pp. 1120–1132. https://doi.org/10.1016/j.egyr.2022.01.031

Saleheen, M.Z., Salema, A.A., Islam, S.M.M., Sarimuthu, C.R. and Hasan, M.Z., 2021. A target-oriented performance assessment and model development of a grid-connected solar PV (GCPV) system for a commercial building in Malaysia, *Renewable Energy*, 171, pp. 371–382. https://doi.org/10.1016/j.renene.2021.02.108

Sharma, A. and Saxena, A., 2024. Statistical error analysis of photovoltaic systems under MPPT control using RMSE and MAPE metrics, *Solar Energy*, 270, P. 112390. https://doi.org/10.1016/j.solener.2024.112390

Skoplaki, E. and Palyvos, J.A., 2009. Temperature dependence of photovoltaic module performance, *Solar Energy*, 83(5), pp. 614–624.

Tey, K.S. and Mekhilef, S., 2023. Modified incremental conductance MPPT algorithm to mitigate steady-state oscillations, *Solar Energy*, 252, pp. 28–40. https://doi.org/10.1016/j.solener.2023.01.012

Villalva, M.G., Gazoli, J.R. and Filho, E.R., 2009. Comprehensive modeling and simulation of photovoltaic arrays, *IEEE Transactions on Power Electronics*, 24(5), pp. 1198–1208.

Youssef, A. and Kanaan, H.Y., 2024. Performance benchmarking of low-power photovoltaic systems under MPPT operation in hot climates, *Energy Reports*, 10, pp. 4121–4134. https://doi.org/10.1016/j.egyr.2024.02.067

التقييم العددي والتجريبي لأداء MPPT في نظام PV بقدرة 50 واط باستخدام وحدة التحكم 2440ML في شحن الطاقة الشمسية

إيناس غزوان فيصل *، شيماء علاء الدين مهدي، عماد طالب هاشم

قسم الطاقة، كلية الهندسة، جامعة بغداد، بغداد، العراق

الخلاصة

تُقدم هذه الدراسة تحقيقًا تجريبيًا وعدديًا مشتركًا لأداء لوح شمسي بقدرة 50 واط باستخدام وحدة التحكم 2440ML لتتبع نقطة القدرة القصوى (MPPT) تحت ظروف إشعاع شمسي مختلفة وأحمال مقاومية متنوعة. تم تحليل ثلاث حالات تشغيل: بدون تتبع، وحمل مقاومة بقيمة 90 أوم، وآخر بقيمة 115 أوم. تم حساب القدرة النظرية والكفاءة باستخدام بيانات الإشعاع الشمسي ودرجة حرارة اللوح وخصائص الوحدة، ومقارنتها بالنتائج التجريبية لتقييم دقة النموذج وفعالية وحدة التحكم. سُجلت أعلى قدرة خرج تجريبية بلغت 49.70 واط عند إشعاع 1000 واط/م² باستخدام مقاومة 115 أوم، متقاربة جدًا مع القدرة النظرية البالغة 50.30واط، بنسبة خطأ نسبي لم تتجاوز .1.2% أما حالة عدم التتبع، فقد حققت قدرة قصوى قدرها 46.51 واط، مع انحراف ملحوظ عن القيم النظرية .أظهر تحليل الجذر التربيعي لمتوسط الخطأ (RMSE) أن حالة عدم التتبع سجلت أعلى القيم (7.92 واط للقدرة، و2.84% للكفاءة)، في حين سجلت حالتا 90 أوم و115 أوم قيمًا أقل بشكل ملحوظ (4.12 واط و1.87% على التوالي). تؤكد هذه النتائج فعالية وحدة التحكم 2440ML في تحسين أداء النظام الشمسي من خلال التتبع الأمثل لنقطة القدرة القصوى، كما تُثبت دقة النموذج العددي المُطور كأداة موثوقة لتقييم وتحليل أداء الأنظمة الكهروضوئية.

الكلمات المفتاحية: الإشعاع الشمسي، درجة حرارة الوحدة، الحمل المقاوم، تتبع نقطة القدرة القصوى

Appendix

Table A1. Maximum power point of solar charger controller (ML2440)

Battery type	Rechargeable, 2500mAh (1.5V) * 8	
AC Adaptor	AC 110V or 220V input DC 12V/1~3A output	
Dimension	257(L) * 155(W) * 57(H) mm	
Weight	1160g	
Operation environment	0 °C - 50 °C, 85% RH (relative humidity)	
Temperature coefficient	0.1% of full scale/ °C (< 18 °C or > 28° C)	
Storage environment	-20° C ~ 60 °C, 75% RH	
Accessories	User manual * 1, AC adaptor*1 Optical USB cable*1 Software CD *1, software manual *1 Kelvin clips(6A max) *1 set	
DC voltage measurements		
Range	**Resolution**	**Accuracy**
0-6	0.001V	±1% ±(1% of V_{open}±9 mV)
6-10 V	0.001V	±1% ±(1% of V_{open}±0.09 V)
10-60 V	0.01 V	±1% ±(1% of V_{open}±0.09 V)
DC current measurements		
Range	**Resolution**	**Accuracy**
0.01-6 A	0.1mA	±1% ±(1% of $I_{short\ n}$±0.09 mA)
0.6-61A	0.1mA	±1% ±(1% of $I_{short\ n}$±0.09 mA)
1-6 A	1mA	±1% ±(1% of $I_{short\ n}$±0.09 mA)

Table A2. Measurement Systems, Instruments, and Equipment Used in the Experimental Setup

Category	Device/ System	Manufacturer	Model Number	Serial Number	Purpose
Environmental Monitoring System	Wireless Weather Sensor with GPS	PASCO Scientific	PS-3200	Not available	Measurement of solar irradiance, ambient conditions, and location data
Power Control System	MPPT Solar Charge Controller	EPEVER	ML2440	Not specified by manufacturer	Maximum power point tracking and PV operating point regulation
Electrical Measurement Instrument	Solar Module Analyzer	PROVA Instruments Inc.	PROVA 210A	Not available	Acquisition of I–V and P–V characteristics and maximum power point identification
Load System	Resistive Load Bank	Laboratory Equipment	Fixed resistors (90 Ω, 115 Ω)	Not applicable	Load matching and performance evaluation under controlled resistance values

Note: Serial numbers of the listed instruments were not available during the experimental work. All systems and measurement instruments were calibrated prior to experimentation in accordance with standard laboratory calibration procedures, ensuring measurement reliability and reproducibility.